THE JOURNAL OF PHYSICAL CHEMISTRY C

Article

pubs.acs.org/JPCC

Dynamics of the Photogenerated Hole at the Rutile TiO_2(110)/Water Interface: A Nonadiabatic Simulation Study

Georgios A. Tritsaris,[†] Dmitry Vinichenko,[‡] Grigory Kolesov,[†] Cynthia M. Friend,[‡] and Efthimios Kaxiras*[,†,§]

[†]School of Engineering and Applied Sciences, [‡]Department of Chemistry and Chemical Biology, and [§]Department of Physics, Harvard University, Cambridge, Massachusetts 02138, United States

Supporting Information

ABSTRACT: Hydrogen production in photoelectrochemical cells constitutes an important avenue toward carbon-free fuel. The most convenient process for hydrogen production is the splitting of water molecules, which necessitates a catalytic reaction involving a semiconductor. Here, we introduce a framework for the study of photocatalyzed reactions on semiconductor surfaces based on time-dependent density functional theory that explicitly accounts for the evolution of electronically excited states. Within this framework, we investigate the possibility of hole-mediated splitting of molecularly adsorbed water on a representative metal oxide surface—the rutile TiO_2(110). We find that oxidative dehydrogenation of water is possible in synergy with thermal effects at temperatures between 60 and 100 K only when defects like Ti interstitials are present in the subsurface region. This study presents a general computational strategy for describing photoexcited semiconductor/adsorbate interfaces and also demonstrates that the occurrence of water dissociation on the rutile TiO_2(110) surface depends sensitively on the local atomic environment and external parameters such as temperature.

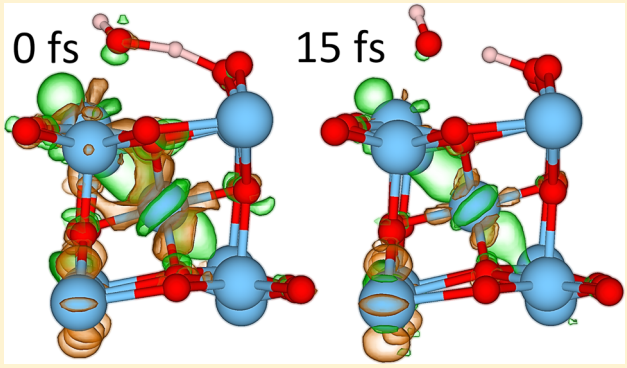

INTRODUCTION

Light-assisted hydrogen production in photoelectrochemical cells (PECs) constitutes an avenue toward solar energy conversion for the production of carbon-free fuel.[1] Upon illumination the oxygen evolution reaction (water oxidation reaction) occurs on the anode electrode, which can be described by the overall reaction

$$2H_2O + 4h^* \rightarrow O_2 + 4H^+$$

with hydrogen being evolved on the cathode. The conversion efficiency of the PEC depends critically on the catalytic performance of the electrodes. Nanostructured devices based on titanium dioxide (TiO_2) are promising candidates for wide use in photon-induced reactions because of this material's photochemical stability, nontoxicity, and natural abudance.[2−6] TiO_2 is a semiconductor metal oxide with an optical band gap of ∼3.2 eV in its bulk rutile form and band gap edges that straddle the water redox potentials; that is, the involved chemical reactions become thermodynamically accessible upon photon absorption. The catalytic activity of TiO_2 can be enhanced by cocatalysts or by metal dopants or defects due to ambient contamination during catalyst preparation.[7−11] The effect of such structural modifications on the thermochemistry at the surface/adsorbate interface has been discussed extensively in the literature,[3,5,12] but a comprehensive atomistic description of dynamic processes, such as the transport of the photogenerated charge carriers in the surface, is lacking even for pure TiO_2. Photon-induced water dissociation on the rutile TiO_2(110) surface has recently been reported in the scanning tunneling microscope study of Tan et al.,[13] which demonstrated a very low rate (few events per hour) O−H bond-breaking in water upon irradiation with ultraviolet (UV) light under ultrahigh-vacuum conditions at 80 K. However, according to density functional theory (DFT) calculations reported by Patel et al.,[14] the highest occupied molecular orbitals of molecular water are 1.40 eV below the valence band maximum (VBM) of the surface, which raises the question whether the reported dissociation of water is light-driven.

The measured properties of real materials depend on the preparation methods and conditions, which makes the identification of universal structure−property relationships a challenging task and hinders a systematic approach to catalyst optimization. Atomistic modeling and simulation of surface/adsorbate interfaces can provide insights into the microscopic physicochemical processes that control catalysis,[12,15−17] an inherently atomic-scale phenomenon, as well as interfacial charge-carrier transfer.[18−20] Previous theoretical studies of photon-mediated catalysis on rutile TiO_2 surfaces used

Received: August 24, 2014
Revised: November 3, 2014
Published: November 6, 2014

   dx.doi.org/10.1021/jp508557w | J. Phys. Chem. C 2014, 118, 27393−27401

ground-state calculations to investigate the effect of excited electronic states on reaction energetics and neglected the details of charge-carrier motion which can strongly affect the overall reaction rate. This highlights the need for computational methods to investigate charge-carrier dynamics in materials accurately and realistically.[21−23] Here we use *ab initio* electronic structure calculations within DFT[24] and its time-dependent version (TDDFT)[25] to develop a framework based on the concept of localized and delocalized electronic states for the study of photocatalytic reactions on semiconductor surfaces. Within this framework we evaluate the possibility of splitting of molecularly adsorbed water by photogenerated holes on rutile TiO_2 surfaces with (110) orientation, which provides insights at the femtosecond time scale (10^{-15} s). In addition, the time-domain description of the interaction of the hole with the water molecule could elucidate the reaction mechanism of other photochemical reactions where water is present.

From our simulations we find that whether the first step of water dissociation is photon-induced or thermal depends sensitively on the local atomic environment and external parameters such as temperature. Specifically, oxidative dehydrogenation of molecular water by a photogenerated hole is possible in synergy with thermal effects only on surfaces with defects, such as subsurface interstitial Ti atoms which act as trap sites for the hole. Our explicit time-dependent modeling provides useful guidelines for the rational design of efficient light-driven catalysis through careful control of the active site on the surface.

MODELS AND METHODS

TiO_2 in its rutile form is a tetragonal crystal in the crystallographic space group $P4_2/mnm$ (No. 136) and has 2 formula units in the unit cell. Its most stable low-index surface is the one with (110) orientation (the calculated surface energy for the relaxed surface is 15.6 meV/au^2).[26] We used a unit cell of 2 Ti and 4 O atoms to model the bulk structure of rutile TiO_2 and an extended, 4 trilayer thick slab containing 162 atoms to model the (110) surface (Figure 1). The latter was

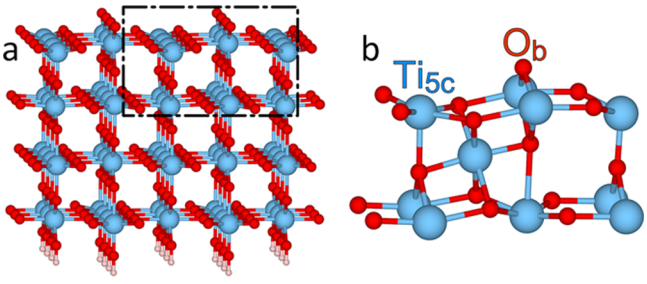

Figure 1. Structural model of the rutile TiO_2 surface with (110) orientation. Blue, red, and white spheres represent Ti, O, and H atoms, respectively. (a) Simulation cell of the stoichiometric surface with nearest O atoms in the surface plane. (b) A portion of the simulation cell, identified by the dashed area in (a), with a Ti interstitial defect in the subsurface region. The surface 5-fold coordinated Ti atom (Ti_{5c}) and bridging O atom (O_b) are identified.

constructed by trunctation of the bulk structure along the (110) crystallographic plane. The obtained unit cell was augmented by a void region with width 8 Å on each side of the slab (z-direction) to ensure that the wave functions vanish smoothly away from the surface along the nonperiodic direction, as would be required in a model of the isolated system. To model the catalyst surface, we used supercells with (3×2) periodicity relative to the primitive unit cell. One side of the slab was terminated with additional hydrogen atoms (bonded to the exposed O atoms) and hydroxyl (−OH) ions (bonded to the exposed Ti atoms) in order to eliminate spurious localized states associated with the dangling bonds of O and Ti atoms, respectively, and emulate the bulk region of the catalyst. The positions of all atoms were optimized while keeping the lateral dimensions of the unit cell fixed to the corresponding bulk values and the terminating −OH groups constrained in the direction perpendicular to the surface.

We performed total energy calculations using the GPAW code,[27] a grid-based implementation of the projected augmented-wave (PAW) method for all-electron calculations within the frozen core approximation.[28] The PAW setup for Ti (O) accounts for 12 (6) valence electrons and 10 (2) electrons in the frozen core (GPAW setup release 9672). A real-space grid with spacing of 0.18 and 0.24 Å was used for static and time-dependent calculations, respectively, and the reciprocal space was sampled only on the Γ-point because of the large lateral dimensions of the supercell. We used the Perdew−Burke−Ernzerhof (PBE) functional to describe exchange and correlation in the electronic system.[29] Because of the inadequate description of the strong Coulomb repulsion between semicore 3d electrons localized on Ti, the PBE functional was augmented with the Hubbard-like term[30] $\sum_\alpha E^\alpha_{\mathrm{orb}}$ with $E^\alpha_{\mathrm{orb}} = (U_{\mathrm{Ti(d)}}/2)[\mathrm{Tr}(\hat{\rho}^\alpha) - \mathrm{Tr}([\hat{\rho}^\alpha]^2)]$, following the rotationally invariant formulation of Dudarev et al.,[31] where $\hat{\rho}^\alpha$ is the atomic orbital occupation matrix of the 3d orbital of the Ti atom α and $U_{\mathrm{Ti(d)}}$ is an effective parameter quantifying the screened Coulomb electron−electron interaction. This so-called DFT+U approach has been shown to describe trends in surface reactivity on TiO_2 with satisfactory accuracy compared to experiment[10,30,32] and with much less computational effort compared to approaches that use hybrid exchange and correlation functionals, which apply the same correction to the entire system regardless of where the error originates from.

To obtain electronic configurations at the moment of vertical excitation, an electron is promoted to the bottom of the conduction band described by the wave function ψ_{N+1}, and we use a generalization of the Δ self-consistent field method (Δ SCF) to allow the hole occupy specifically designed linear combinations of the N occupied Kohn−Sham wave functions.[33] This maintains charge neutrality in the total system. The high dielectric constant of rutile TiO_2 (∼100) contributes to the screening of opposite charges from each other. The electron density, $n(r)$, at each self-consistency cycle is calculated from[33]

$$n(r) = \sum_{i=1}^{N} \psi_i^*(r)\psi_i(r) - \sum_{i,j=1}^{N} a_i^* a_j \psi_i^*(r)\psi_j(r) + \psi_{N+1}^*(r)\psi_{N+1}(r)$$

The expansion coefficients, α_i, are optimized in a self-consistent manner so that the orbitals associated with the hole and electron (second and third terms in the expression for $n(r)$) resemble some input wave functions as much as possible. This approach has been used to study hole localization in rutile and anatase TiO_2, giving results in agreement with published photoluminescence measurements.[34] It has the additional benefit of constructing Kohn−Sham wave functions that are variationally optimized and not involving computationally expensive summations over many unoccupied electronic states, in contrast for example to calculations based on the linear-

dx.doi.org/10.1021/jp508557w | J. Phys. Chem. C 2014, 118, 27393−27401

response TDDFT scheme or the solution of the Bethe–Salpeter equation.

We used the Ehrenfest approximation within the framework of real-time propagation TDDFT to couple the electronic and ionic dynamics in the excited-state catalytic system,[25,35,36] which is evolved from time t to time $t + \Delta t$ using the time-evolution operators $\hat{T}_N$ and $\hat{T}_e$, for the nuclear and electronic parts, respectively:[35]

$$\hat{T}_{N,e}(t, t + \Delta t) = \hat{T}_N(t, t + \Delta t/2)\hat{T}_e(t, t + \Delta t) \times \hat{T}_N(t + \Delta t/2, t + \Delta t)$$

The electronic subsystem is treated quantum mechanically, propagated using the Crank–Nicholson semi-implicit scheme for $\hat{T}_e$ with a predictor-corrector time step of $\Delta t/2 = 5$ as (1 as $=10^{-18}$ s).[37] The forces on the classical ions result from a mean-field average over the electronic states, and the ionic subsystem is evolved in time by application of the standard velocity Verlet propagator, $\hat{T}_N$. The occupation of all the wave functions in the system remains fixed during the simulation. Examples of previous successful applications of Ehrenfest dynamics include the study of charge-carrier transport in dye-sensitized TiO_2 nanowires[38] and hydrogen bombardment of graphene-like nanoflakes,[35] and it is generally expected to work well in situations where the electronic states have similar character. In the present work we use TiO_2 as an illustrative example because of the availability of experimental data, but our computational strategy is general and should be useful for the study of other metal oxides.

In the rutile TiO_2 crystal each Ti (O) atom in the unit cell of the bulk structure has 6 (3) nearest neighbors. After structural optimization of the unit cell of the bulk structure, the calculated lattice constants are a_0 = 4.65 Å and c_0 = 2.96 Å, in good agreement with experiment (the measured lattice constants at 15 K are a_0 = 4.586 Å and c_0 = 2.954 Å)[39] and previous DFT calculations at the PBE approximation level (a_0 = 4.65 Å and c_0 = 2.96 Å).[30] For all calculations in the present work we use $U_{Ti(d)}$ = 4.2 eV to improve the description of electronic screening in TiO_2, as proposed in previous studies using Dudarev's DFT+U approach within the PAW formalism.[21,40] For $U_{Ti(d)}$ = 0 the calculated lattice constants change less than 1%. The outermost atomic layer in the stoichiometric (110) surface exhibits 5-fold coordinated Ti atoms (Figure 1, Ti_{5c}) and 2-fold coordinated O atoms, hereafter referred to as "bridging" O atoms (Figure 1, O_{br}).

In a photoelectrochemical cell, a photon of adequate energy excites an electron in the semiconductor catalytic material to the conduction band, leaving a hole in the valence band. After the photogenerated hole reaches the surface it is transferred to the water molecule, which is oxidized to hydroxyl, assuming that recombination of charge carriers does not occur first (these radiative relaxation processes are not considered in the present work). The lowest energy needed for the creation of an electron–hole pair is determined by the material's optical adsorption edge: according to calculations by Kang and Hybertsen based on the GW approximation to the self-energy and the solution of the two-particle Bethe–Salpeter equation, the energy of the first dipole-allowed singlet exciton is 3.35 eV for bulk rutile TiO_2, almost equal to the quasiparticle band gap, 3.34 eV.[41] Within the framework of the density functional theory, the fundamental band gap of semiconductors and insulators is underestimated, but the DFT+U approach partially alleviates this problem.[12] We calculate the Kohn–Sham band gap of the bulk structure of rutile TiO_2 to be 1.69 eV for $U_{Ti(d)}$ = 0 and 2.33 eV for $U_{Ti(d)}$ = 4.2 eV. For the stoichiometric TiO_2(110) surface, the band gap is calculated to be 1.72 and 2.38 eV for $U_{Ti(d)}$ = 0 and $U_{Ti(d)}$ = 4.2 eV, respectively. Because the conduction band has mainly 3d Ti-orbital character and the valence band 2p O-orbital character, the band gap widens in an asymmetric fashion with increasing $U_{Ti(d)}$ as the CBM shifts to a higher energy.

A single water molecule preferably binds to the surface directly above a Ti_{5c} atomic site; this is supported by experimental evidence from scanning tunneling microscopy studies under ultrahigh-vacuum conditions and theoretical work based on DFT investigations of the interaction between water and the rutile TiO_2(110) surface.[13,32] Upon oxidation of water, one of its H atoms is transferred to TiO_2 where it binds to a bridging O atom, leaving an –OH group adsorbed at the Ti_{5c} site. To quantify the stability of water on the surface, we calculate the binding energy with respect to the clean surface and an isolated molecule. In this scheme, the lower the calculated value of the binding energy, the stronger the adsorption. For the coverage of 1/6 monolayer, adsorption is exothermic, and the calculated binding energy for molecular water is –0.96 eV, 0.22 eV higher than that for dissociated water with a binding energy of –1.18 eV. The lateral dimensions of the supercell ensure no interaction between water molecules adsorbed at neighboring supercells, as it would be relevant to the low-coverage limit. Using nudged elastic band calculations,[42] we find that the minimum-energy barrier for thermal dissociation is relatively low, 0.15 eV (14 kJ/mol). The relative stability of the two modes of adsorption, molecular and dissociative, and the energy barrier depend on the computational method and the details of the structural model employed, for instance, the thickness of the slab, as discussed in the work of Kowalski et al.[14,43] For the structural model of the TiO_2(110) surface employed in our calculations, going from 4 to 5 trilayer thick slabs changes the binding energy for adsorption by only 0.06 eV and the center of the water p O-states, calculated as the first moment of the projected density of states on the O atom, is shifted to lower energy by 0.06 eV. From this test, we do not expect the conclusions of the present work to be affected by computational details such as the thickness of the slab.

After ground-state structural optimization, the temperature of the catalytic system was raised from 0 K to a temperature relevant to experimental conditions.[13] We first assigned initial velocities to the ions of the optimized surface/adsorbate configuration according to the equilibrium Boltzmann–Maxwell distribution at 100 K, and we subsequently performed a molecular dynamics simulation for 300 fs in the micro-canonical ensemble (N, V, E) using a time step of 1 fs. The positions of the atoms in the bottom trilayer were kept fixed during the simulation. We then used an equilibrated configuration from this simulation as the ground state of the surface/adsorbate interface at the moment of the vertical excitation.

To model the excited-state surface/adsorbate interface, the electronic structure of the thermalized configuration was augmented by two wave functions: one to which we assign occupancy of –1 (hole) designed as discussed in the next section, and the other corresponds to the wave function associated with the CBM which is assigned occupancy of +1 (electron). The obtained electron–ion system corresponds to the excited state of the surface/adsorbate interface at the

dx.doi.org/10.1021/jp508557w | J. Phys. Chem. C 2014, 118, 27393–27401

moment of the vertical excitation, which is defined as the zero of the time scale (t = 0). In this work, we concentrate on the interaction of the hole with the adsorbate, and we do not consider exciton generation and diffusion or the separation of the charge carriers that precede hole transport to the surface. Instead, the excitation is represented by a weighted sum over Kohn−Sham wave functions in an electronic configuration that does not necessarily correspond to the initial excitation of the catalytic system by light which leads to exciton generation. The associated vertical excitation therefore may not contribute strongly to a true excitonic state of the surface/adsorbate interface, but investigation of the optical response of the material is beyond the scope of the current study.

Our computational strategy for the study of the dynamics of the interaction between the surface and the molecule under conditions of photoexcitation can be summarized as follows: (1) After ground-state structural optimization, *ab initio* molecular dynamics in the microcanonical ensemble is used to bring the catalytic system to a desired temperature. (2) An excitation is created by promoting an electron from a state which is an expansion of the occupied Kohn−Sham wave functions to the bottom of the conduction band of the surface. (3) The excited-state surface/adsorbate interface is evolved in time using Ehrenfest dynamics within the framework of real-time propagation TDDFT. The evolution of the catalytic system is studied by monitoring the difference in the electron densities between the excited-state system and the ground state of the same ionic configuration at each time instant.

RESULTS

We used three different orbitals for the hole to investigate its motion in the surface, discussed in order of increasing relevance to standard experimental conditions. The first was modeled after a wave function entirely localized at the water molecule adsorbed on the stoichiometric TiO_2(110) surface, chosen because the vertical excitation energy, 9.60 eV, was such that it ensured the dissociation of the water molecule. The main purpose of this excitation was to evaluate the suitability of our methodology for the study of photon-induced dynamic processes at surface/adsorbate interfaces. The second hole wave function was localized at the surface, and the excitation energy was 3.93 eV, close to the band gap of the bulk material, which should correspond to realistic situations for irradiation with UV light. The third excitation energy was 1.00 eV in a configuration that included a hole wave function localized at a subsurface defect near the site of the water molecule absorption. The evolution of these three excited states in time is shown in Figure 2. We discuss them in detail in this order.

In the first excitation, the wave function associated with the hole resembles as much as possible the nonbonding orbital of an isolated water molecule. The difference in energy between the excited and ground state at t = 0 is 9.60 eV (equal to the vertical-excitation energy). This energy is more than 3 times higher than the band gap, and it corresponds to the extreme UV irradiation wavelength of 130 nm. This is because the molecular orbitals of water where the hole was created are energetically much lower than the TiO_2 band gap edges: the center of the water p O-states is 4.72 eV lower than the VBM and 7.09 eV than the conduction band minimum (CBM). It is natural to expect that such high excitation energy can generate a deep hole with the oxidative power to initiate splitting of water. We calculate the difference between the electron density of the

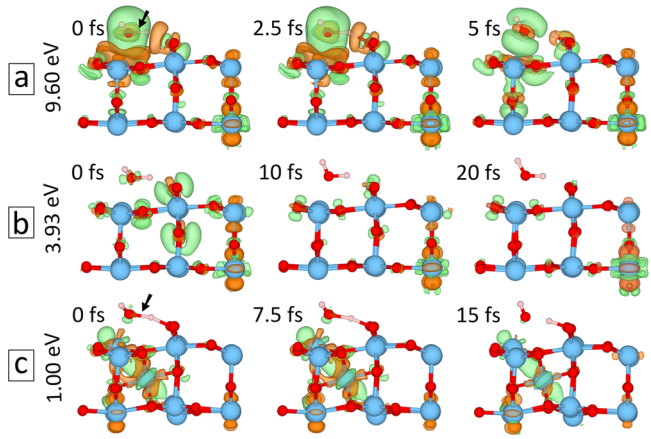

Figure 2. Difference between the electron densities of the excited state and the ground state of the TiO_2(110) surface/water interface for the same ionic configuration at different time instants during simulation for three different vertical excitations: (a) 9.60 eV and (b) 3.93 eV in the stoichiometric surface and (c) 1.00 eV in a defected surface. The electron density differences are shown by isosurfaces with value 0.01 e/Å^3 (e is the charge of the bare electron), where green and orange signify regions of electron charge depletion and charge accumulation, respectively. Black arrows point at the O−H bonds being broken.

excited state and the electron density of the ground state of the same ionic configuration at each instant as a means to monitor the evolution of the excited state electron−ion system (see also supporting information). Figure 2a shows that in comparison to the ground state, charge is depleted mostly in the region around the water O atom (light green) immediately after the vertical excitation (t = 0). It also reveals an image charge in the surface that screens the excitation as well as some charge redistribution within the water molecule and between the molecule and the nearest bridging O atom of the surface. The excess charge introduced by the electron wave function is mostly localized on Ti atoms in the subsurface region and away from the water molecule.

After the high-energy vertical excitation the system is evolved in time using Ehrenfest dynamics. Similar to the situation at t = 0, at t = 2.5 fs the hole is almost entirely localized on the water molecule, although some charge has also been depleted from the O atom in the subsurface region nearest to the water molecule. At t = 5 fs the water molecule has dissociated, leaving one −OH group bound to the Ti_{5c} atomic site (Figure 2a), and at t = 10 fs the hole has been transferred to the subsurface O atom and the charge distribution associated with the hole resembles the p_z O-orbital (with two lobes aligned in the direction perpendicular to the surface). Part of the potential energy, about 2.7 eV, of the initial excitation is lost through energy transfer to the ionic motion. The distance between the O atom of the water molecule and the H atoms increases from 1.05 Å at t = 0 to 1.21 Å at t = 2.5 fs and to 1.62 Å at t = 5 fs. The distance between the H atom of the water molecule and the nearest bridging O atom decreases from 1.52 Å at t = 0 to 1.35 Å at t = 2.5 fs and to 0.94 Å at t = 5 fs. Inspection of Figure 2a also reveals that during the entire simulation time the electron is virtually immobile.

The next vertical excitation we considered, 3.93 eV (see Figure 2b), involves electronic states only near the band gap edges of the surface, which is relevant to experimental UV conditions. In photon-induced catalysis the charge carrier needs to reach the surface/adsorbate interface and to be stable until

dx.doi.org/10.1021/jp508557w | J. Phys. Chem. C 2014, 118, 27393−27401

transferred to the adsorbate.[5] In this respect, carrier trapping is an important issue in interfacial charge transfer, but the possible location of hole traps in the TiO_2 surface remains a subject of investigation, although bridging and subsurface O atoms have been suggested as likely atomic sites for small polarons.[5,44,45] We also found these O atomic sites to mediate hole transport (Figure 2a, t = 5 fs). In order to better understand the effect of spatial localization of charge on the surface/adsorbate interaction, we analyze the electron localization function (ELF) which has proven useful in studying bonding in extended and molecular systems in a chemically intuitive way.[46,47] The ELF is a positive quantity between 0 (blue regions in Figure 3a) and 1 (red regions in Figure 3a), used as a measure of finding an electron in the vicinity of another electron of the same spin (and therefore of the probability of opposite-spin pairs). Figure 3a portrays a two-dimensional cross section of the ELF through a bridging O atom. In the interior of the slab, the Ti−O has strong ionic character as evidenced by the high localization values, >0.8, near each O atom, as would be expected in the bulk structure of TiO_2. For the exterior of the slab, in contrast to the bottom surface that is terminated with −OH ions, the top surface also exhibits high ELF values above the bridging O atoms, the signature of a dangling bond. While ELF provides insights into the spatial distribution of chemical bonds, it does not reveal the shape of orbitals where the electrons are expected to exist. To this end, we analyze the maximally localized Wannier functions of the valence band manifold, an approach which allows the representation of extended Bloch states with atomic-like orbitals.[48] We used the Wannier90 utility interfaced to the Quantum Espresso code to produce the Wannier functions.[48]

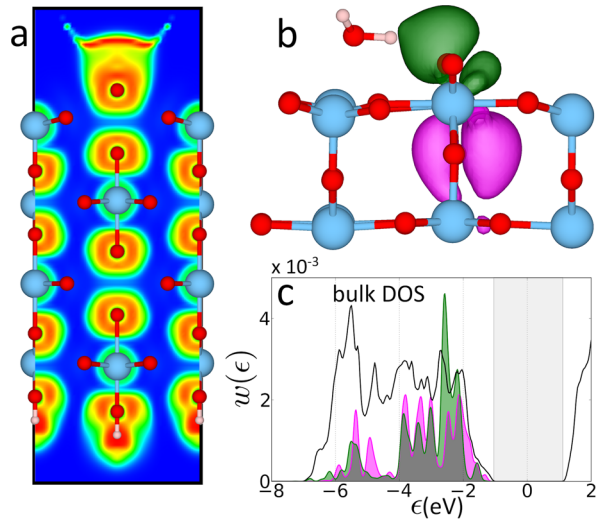

Figure 3. (a) Two-dimensional cross section of the electron localization function through the bridging oxygen (blue, green, and red for values of 0, 0.5, and 1). (b) Isosurfaces representing the maximally localized Wannier functions spanning the range of energies closest to the valence band maximum for the bridging (green cloud) and subsurface (violet cloud) oxygen atoms nearest to the water molecule. (c) Projections, $U_{Ti(d)}$, of the Wannier functions onto the Kohn−Sham states of the TiO_2(110) surface (the regions where green and violet weights overlap appear gray). The total area of each shaded plot equals 1. The black line marks the density of states of the bulk, and the middle of its band gap is defined as the zero of the energy scale. The shaded vertical strip delimits the band gap.

The functions we obtained possess the expected character: in the bulk-like region of the slab, there is one Wannier function for each σ bond between Ti and O atoms and in the subsurface one "lone pair" orbital on each of the O atoms (represented by the purple clouds in Figure 3b). On the surface, each bridging O atom has a dangling bond which mixes with the lone pair, resulting in two almost equivalent Wannier functions (one of which is shown by the green clouds in Figure 3b). Because the Wannier functions are linear combinations of the eigenfunctions of the Kohn−Sham Hamiltonian, they can be represented by the weights of the Kohn−Sham orbitals contributing to a given function. We find that the Wannier function corresponding to the dangling bonds of the bridging O atom is comprised mostly of the Kohn−Sham orbitals that span the range of energies near the top of the valence band (Figure 3c). These Wannier functions were used as a guide for modeling a hole wave function that is equally distributed over the bridging and subsurface O atoms nearest to the water molecule. In order to accomplish this spatial distribution of the hole wave function in ΔSCF, we calculated the projections of the Wannier function on the atomic orbitals; the largest coefficients that correspond to the s and p O-orbitals are presented in Table 1.

Table 1. Coefficients Corresponding to the Contribution of s and p O-Orbitals to the Wannier Functions Localized at the Bridging and Subsurface O Atom Nearest the Adsorbed Water Molecule

	O-orbital			
atomic site	s	p_x	p_y	p_z
bridging oxygen	0.32	0.10	0.10	0.05
subsurface oxygen	0.09	0.07	0.06	0.05

Using the previously thermalized ionic configuration, we model the excitation at t = 0 by augmenting the electronic system with a wave function which is a linear combination of the PAW atomic partial waves according to Table 1 and which resembles as much as possible the calculated Wannier functions shown in Figure 3b. As in the case of the high-energy excitation (vertical-excitation energy of 9.60 eV), the electron wave function corresponds to the state at the CBM. Upon excitation, charge is depleted from the region in the vicinity of the bridging and subsurface O atoms that are nearest to the water molecule, and there is also some redistribution of charge in the molecule and at the surface O atoms (Figure 2b, t = 0). The vertical-excitation energy, 3.93 eV, corresponds to photon wavelength of 313 nm, which lies within the typical range for irradiation with UV light in experiment.[6]

This low-energy excitation involves no bond-breaking events during the first 30 fs. We do not expect that propagation of the electron−ion system at longer times would lead to oxidation of water since already at 10 fs the hole has diffused to the interior of the slab. This is because the net positive charge at the surface/adsorbate interface gives rise to a gradient in the electrostatic potential that drives the hole away from the water molecule.[45] Irrespective of the role of ionic motion, hole transport is mediated by atomic O sites through transitions involving electronic states with strong p O-level contribution. The strong coupling between these atomic sites prevents the spatial confinement of the hole near the water molecule, and the initially localized redistribution of the electron density at t = 0 spreads over the entire lattice supercell (which comprises several primitive unit cells) within a few femtoseconds. Most

dx.doi.org/10.1021/jp508557w | J. Phys. Chem. C 2014, 118, 27393−27401

importantly, although there is considerable overlap between the oxide surface and molecular O states at lower energies in the −6 to −2 eV range relative to the VBM, there are no molecular states near the band gap edge where the hole could reside as the projected density of states plot in Figure 4 reveals.[14] For the

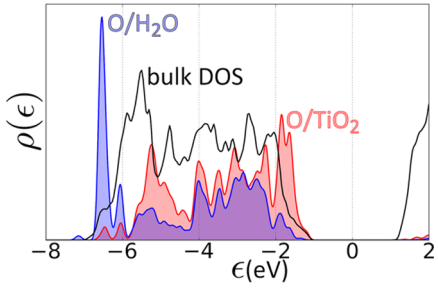

Figure 4. Density of states projected onto the p orbitals of the oxygen atoms in the top atomic trilayer of the TiO_2 (110) surface (red) and the oxygen atom of the water molecule (blue) at simulation time of 30 fs after low-energy excitation (3.93 eV). The black line marks the density of states of the bulk (scaled by a factor of 1/72), and the middle of its band gap is defined as the zero of the energy scale.

calculation of the projected density of states we used the time-dependent wave functions, which although do not have a rigorous physical meaning, we used to obtain a qualitative description of the effect of the moving ions on the energy of molecular states. Modeling the orbital associated with the hole after a wave function that is (a) entirely localized at a single bridging O atom, (b) equally distributed over all 6 bridging O atoms in the supercell, or (c) equally distributed over the water molecule (nonbonding orbital) and the nearest bridging O atom, results in delocalization of the hole within 20 fs. Calculations with $U_{Ti(d)}$ = 2.0 eV lead to the same outcome as for $U_{Ti(d)}$ = 4.2 eV. We conclude from our excited-state Ehrenfest dynamics that photon-induced dehydrogenation of molecular water on pure TiO_2(110) surfaces is not likely.

The rutile phase of stoichiometric TiO_2 has for long been of great scientific interest as a prototypical metal oxide. This phase is mostly inert and under standard conditions its surface is substoichiometric with excess Ti atoms.[7] Surface and near-surface local imperfections, such as the common Ti interstitials and O vacancies, modify the surface chemistry of this material and can be beneficial to its efficiency as a catalyst. For example, Ti interstitials in the subsurface region can stabilize the bonding of chemical species as in the case of formadelhyde ($-OCH_2$), discussed in the DFT study of Haubrich et al.[9] In what concerns the reactions of water on the rutile TiO_2 surface, increased interaction with the surface induced by the defects should decrease the energy barrier for thermal dissociation. In addition, defect states reduce the minimum energy for photoexcitation from the UV range to the visible range and can act as local trap sites for the photogenerated hole until it is transferred to the water molecule to promote the oxidation reaction.

Motivated by the above considerations, we studied the role of Ti interstitials in photon-induced water splitting on the rutile TiO_2(110) surface. To model the defected catalytic surface, we introduced a single Ti atom in one of the ⟨110⟩ channels in the subsurface region of our structural model which corresponds to a concentration of 1/6 monolayer of Ti atoms (see Figure 1b). This configuration is thermodynamically more stable (lower in energy) by 0.22 eV compared to a configuration with the Ti interstitial between two ⟨110⟩ channels. The calculated binding energy for molecular water adsorbed on the Ti_{5c} atomic site is −1.12 eV, less stable by 0.15 eV than dissociated water which has an adsorption energy of −1.27 eV, and more stable by 0.16 eV than adsorption on the stoichiometric surface (adsorption energy of −0.96 eV). Moreover, incorporation of the Ti interstitial in the TiO_2 lattice introduces electronic states in the band gap. The calculated energy of these defect-related states depends on the details of the computational method, for instance the value of the parameter U in the DFT+U approach.[30,49] For $U_{Ti(d)}$ = 4.2 eV the defect-induced state is 1.00 eV below the CBM, in reasonable agreement with UV photoelectron spectroscopy on bulk reduced rutile TiO_2 which reveals defect-related electronic states at about 0.9 eV below the CBM.[50] Ti interstitials in the subsurface region also result in a lower energy barrier for thermal subtraction of hydrogen from water. During ground-state molecular dynamics in the micro-canonical ensemble at 100 K, we find that an adsorbed water molecule spontaneously dissociates in the presence of a subsurface Ti interstitital, which suggests that the first step of water splitting on defect-containing TiO_2(110) surfaces can be an entirely thermally driven process even at relatively low temperatures. On the other hand, an adsorbed water molecule remains intact at a temperature of 60 K. A resonance between the two limiting structures of molecular and dissociated water occurs at the intermediate temperature of 80 K, and although no thermal dissociation is observed, for 28% of the total simulation time the water O−H bond is elongated more than 10% of its equilibrium value, 1.02 Å, and is elongated by more than 20% of its equilibrium value for 12% of the total simulation time. This extension of the water O−H bond allows the H atom to be shared between the water and bridging O atoms. For comparison, in a simulation at 60 K this bond is never stretched by more than 15%.

To investigate the effect of photoexcitation on water dissociation in the defect-containing surface at 80 K, we considered the situation where an electron is promoted at t = 0 from a defect-related state in the band gap to the CBM (shown in Figure 2c). This corresponds to an excited-state configuration within a polaronic description of a hole trapped by a defect, following irradiation with light of energy equal to or higher than the optical absorption edge of the material. At t = 0, the distance between the water O and H atoms is 1.27 Å and the distance between the water H and bridging O atoms is 1.24 Å. Figure 2c shows that the hole is localized in the subsurface region at the Ti interstitial and partly overlaps the extended form of molecular water. The pinning of the hole near the surface weakens the restorative force on the H atom in the stretched water O−H bond, which leaves the H atom with enough kinetic energy to overcome the energy barrier for approaching the bridging O atom and binding to the surface within 15 fs.

Ehrenfest dynamics is a semiclassical method that cannot capture quantum mechanical processes in the ionic subsystem. Upon including nuclear quantum effects a water H atom could hop onto the nearby bridging O atom at small separations (less than ∼0.2 Å) between the water H and surface bridging O atoms. However, a more complete quantum-mechanical treatment, for example using surface hopping techniques,[51,52] remains currently impractical for the study of our structural models because of size and time scale considerations.

dx.doi.org/10.1021/jp508557w | J. Phys. Chem. C 2014, 118, 27393−27401

DISCUSSION AND CONCLUSIONS

Our results for the interaction of low concentrations of molecular water with stoichiometric and defected surfaces of rutile TiO_2 with (110) orientation have important implications for the photocatalytic activity of the material. We can draw as a first conclusion that whether water photooxidation is possible depends on the local atomic environment and experimental conditions. On the idealized stoichiometric surface a hole relaxed at the top of the TiO_2 valence band cannot oxidize molecularly adsorbed water as the highest occupied molecular orbitals remain lower in energy than the VBM of the surface by −2 eV (Figure 4). Moreover, according to our molecular dynamics simulations, thermal dissociation does not occur at temperatures at least as high as 300 K. Increasing the coverage of water on the surface from 1/6 to 1/3 of a monolayer with two water molecules adsorbed on adjacent Ti_{5c} atomic sites has little effect on the electronic structure of the surface/adsorbate interface due to the weak interaction between the molecules (adsorption is stabilized by 2%). However, our model assumes ultrahigh vacuum, and the effects of complex environments such as electrolytes on the dynamics of the surface/adsorbate interface merit further investigation.[53]

As a second conclusion, we find that the water photooxidation reaction could occur on surfaces containing Ti interstitials at temperatures between 60 and 100 K. In the work of Tan et al.,[13] which reported water photooxidation, the pertinent scanning tunneling measurements were performed at a temperature of 80 K, a critical factor for photocatalytic dissociation according to our findings, in the presence of Ti interstitial defects (a feature not discussed in that work). Because the Ti interstitial participates in the reaction mechanism by modifying the potential energy landscape and by pinning the hole near the surface, the catalytic active site comprises both the Ti_{5c} and Ti-interstitial atomic sites. We calculated that the hopping of a Ti interstitial between two adjacent equivalent equilibrium sites requires overcoming an energy barrier of 0.52 eV (50 kJ/mol). From this fact, we expect that diffusion of Ti interstitials will be of secondary importance regarding the reaction mechanism of water oxidation at temperatures of practical interest. Care must be taken for the correct interpretation of our findings, which demonstrate the importance of thermal effects in water dissociation but the estimated short time for O−H bond breaking, 15 fs, is not necessarily in quantitative correspondence with experimentally measured high rate. In contrast, as a number of necessary conditions must be met for the reaction to occur, the dissociation probability should be low, in support of the observation that rutile TiO_2(110) surfaces are inefficient as catalysts for the water photooxidation reaction under ultrahigh-vacuum conditions.[54] In addition, subsurface defects can act as recombination centers with adverse effects on the dissociation probability, but recombination of charge carriers is not considered in this work. In the same vein, the temperature window which favors a resonant state of adsorption will depend on the structural details of the surface, although the estimated temperature of 80 K is in agreement with experiment.[13]

The interstitial-containing surface studied here can be thought of as a structural model of catalytic surfaces where a hole is trapped at the active site facilitating the reaction. This result highlights the importance of defects in photocatalysis and suggests that careful control of the atomic structure and composition of the surface can enhance the reaction rate. For example, structural defects such as steps or kinks fit a generalized notion of a defect-containing active center,[54−56] but further work is necessary in order to explore how morphologies other than extended flat surfaces mediate photon-induced catalysis.[57]

Our methodology should also be useful for the study of adsorbates other than water. Although the alignment between the electronic levels of the TiO_2 and molecular water is not favorable for the oxidation reaction to occur on the pure and flat (110) surface, the outcome of illumination can be different for species that chemisorb on the surface, such as methoxy ($-OCH_3$). The methoxy radical is a possible reaction intermediate of another important reaction—the methanol oxidation reaction.[58,59] In our initial investigation of this system, the projected density of states calculation reveals that there is a significant population of methoxy O states at the VBM of TiO_2, and therefore methoxy should act as a hole scavenger enabling interfacial hole transfer. A more detailed investigation and analysis are the subject of ongoing work.

In conclusion, we developed a simple methodology for the modeling and simulation of dynamic processes at excited-state interfaces which we used to study charge-carrier motion and interaction with molecularly adsorbed water on rutile TiO_2(110) surfaces. We found that water photooxidation to hydroxyl is possible in synergy with thermal effects. On the stoichiometric surface there are no electronic states associated with water near the VBM of the TiO_2 surface, and therefore oxidation by a photogenerated hole is not possible for excitation energies corresponding to the band gap of TiO_2. By contrast, Ti interstitials in the subsurface region increase the binding strength of water on the surface, lower the minimum energy barrier for thermal dissociation of water, and act as trap sites for holes until they are transferred to water and oxidize it. Moreover, the reaction pathway critically depends on external conditions such as temperature. On the defected surface, low temperatures (<60 K, according to our molecular dynamics simulation) favor molecularly adsorbed water and higher temperatures (>100 K) favor dissociated water. Intermediate temperatures, ∼80 K, favor a resonant state of adsorption that enables splitting of the molecule. Under these circumstances thermal and photon-induced effects act in a complementary manner that leave an ambiguity in the causal sequence: water dissociation can be equally considered a photon-induced and thermal process or a thermal and photoassisted process. Although optimization of catalytic performance is ultimately a combinatorial challenge, this work paves the way for the investigation of the kinetics of photoelectrochemical reactions on semiconductor surfaces and provides useful guidelines for the rational design of efficient photocatalytic materials by careful control of the active sites on the surface.

ASSOCIATED CONTENT

Supporting Information

Animations of hole transport in the surface/adsorbate interface for three different vertical excitations. This material is available free of charge via the Internet at http://pubs.acs.org.

AUTHOR INFORMATION

Corresponding Author

*E-mail kaxiras@physics.harvard.edu (E.K.).

Notes

The authors declare no competing financial interest.

■ ACKNOWLEDGMENTS

The authors thank Till Cremer and Fanny Hiebel for the helpful discussions. G.T. gratefully acknowledges financial support by the SEAS Dean's TomKat Fund for renewable energy research. Computations were performed on the Extreme Science and Engineering Discovery Environment (XSEDE), which is supported by National Science Foundation Grant OCI-1053575, and on the Odyssey cluster, supported by the FAS Science Division Research Computing Group at Harvard University.

■ REFERENCES

(1) Walter, M. G.; Warren, E. L.; Mckone, J. R.; Boettcher, S. W.; Mi, Q.; Santori, E. A.; Lewis, N. S. Solar Water Splitting Cells. *Chem. Rev.* **2010**, *110*, 6446−6473.
(2) Fujishima, A.; Honda, K. Electrochemical Photolysis of Water at a Semiconductor Electrode. *Nature* **1972**, *238*, 37−38.
(3) Fujishima, A.; Zhang, X.; Tryk, D. A. TiO_2 Photocatalysis and Related Surface Phenomena. *Surf. Sci. Rep.* **2008**, *63*, 515−582.
(4) Ni, M.; Leung, M. K. H.; Leung, D. Y. C.; Sumathy, K. A Review and Recent Developments in Photocatalytic Water-Splitting Using for Hydrogen Production. *Renew. Sustain. Energy Rev.* **2007**, *11*, 401−425.
(5) Henderson, M. A. A Surface Science Perspective on Photocatalysis. *Surf. Sci. Rep.* **2011**, *66*, 185−297.
(6) Henderson, M. A.; Lyubinetsky, I. Molecular-Level Insights into Photocatalysis from Scanning Probe Microscopy Studies on TiO_2(110). *Chem. Rev.* **2013**, *113*, 4428−4455.
(7) Diebold, U. The Surface Science of Titanium Dioxide. *Surf. Sci. Rep.* **2003**, *48*, 53−229.
(8) Thompson, T. L.; Yates, J. T. Surface Science Studies of the Photoactivation of TiO_2-New Photochemical Processes. *Chem. Rev.* **2006**, *106*, 4428−4453.
(9) Haubrich, J.; Kaxiras, E.; Friend, C. M. The Role of Surface and Subsurface Point Defects for Chemical Model Studies on TiO2: A First-Principles Theoretical Study of Formaldehyde Bonding on Rutile TiO_2(110). *Chem.—Eur. J.* **2011**, *17*, 4496−4506.
(10) García-Mota, M.; Vojvodic, A.; Abild-Pedersen, F.; Nørskov, J. K. Electronic Origin of the Surface Reactivity of Transition-Metal-Doped TiO_2(110). *J. Phys. Chem. C* **2013**, *117*, 460−465.
(11) Su, R.; Tiruvalam, R.; Logsdail, A. J.; He, Q.; Downing, C. A.; Jensen, M. T.; Dimitratos, N.; Kesavan, L.; Wells, P. P.; Bechstein, R.; et al. Designer Titania-Supported Au-Pd Nanoparticles for Efficient Photocatalytic Hydrogen Production. *ACS Nano* **2014**, *8*, 3490−3497.
(12) Liao, P.; Carter, E. A. New Concepts and Modeling Strategies to Design and Evaluate Photo-Electro-Catalysts Based on Transition Metal Oxides. *Chem. Soc. Rev.* **2013**, *42*, 2401−2422.
(13) Tan, S.; Feng, H.; Ji, Y.; Wang, Y.; Zhao, J.; Zhao, A.; Wang, B.; Luo, Y.; Yang, J.; Hou, J. G. Observation of Photocatalytic Dissociation of Water on Terminal Ti Sites of TiO_2(110)-1 × 1 Surface. *J. Am. Chem. Soc.* **2012**, *134*, 9978−9985.
(14) Patel, M.; Mallia, G.; Liborio, L.; Harrison, N. M. Water Adsorption on Rutile TiO_2(110) for Applications in Solar Hydrogen Production: A Systematic Hybrid-Exchange Density Functional Study. *Phys. Rev. B* **2012**, *86*, 045302.
(15) Tritsaris, G. A.; Rossmeisl, J. Methanol Oxidation on Model Elemental and Bimetallic Transition Metal Surfaces. *J. Phys. Chem. C* **2012**, *116*, 11980−11986.
(16) Tritsaris, G. A.; Greeley, J.; Rossmeisl, J.; Nørskov, J. K. Atomic-Scale Modeling of Particle Size Effects for the Oxygen Reduction Reaction on Pt. *Catal. Lett.* **2011**, *141*, 909−913.
(17) Nørskov, J. K.; Bligaard, T.; Rossmeisl, J.; Christensen, C. H. Towards the Computational Design of Solid Catalysts. *Nat. Chem.* **2009**, *1*, 37−46.
(18) Duncan, W. R.; Prezhdo, O. V. Theoretical Studies of Photoinduced Electron Transfer in Dye-Sensitized TiO_2. *Annu. Rev. Phys. Chem.* **2007**, *58*, 143−184.
(19) Meng, S.; Kaxiras, E. Real-Time, Local Basis-Set Implementation of Time-Dependent Density Functional Theory for Excited State Dynamics Simulations. *J. Chem. Phys.* **2008**, *129*, 054110.
(20) Onda, K.; Li, B.; Zhao, J.; Jordan, K. D.; Yang, J.; Petek, H. Wet Electrons at the H_2O/TiO_2(110). *Surf. Sci.* **2005**, *308*, 1154−1158.
(21) Ji, Y.; Wang, B.; Luo, Y. Location of Trapped Hole on Rutile-TiO_2(110) Surface and Its Role in Water Oxidation. *J. Phys. Chem. C* **2012**, *116*, 7863−7866.
(22) Valdés, A.; Kroes, G.-J. Cluster Study of the Photo-Oxidation of Water on Rutile Titanium Dioxide (TiO_2). *J. Phys. Chem. C* **2010**, *114*, 1701−1708.
(23) Bernardi, M.; Vigil-Fowler, D.; Lischner, J.; Neaton, J. B.; Louie, S. G. Ab Initio Study of Hot Carriers in the First Picosecond after Sunlight Absorption in Silicon. *Phys. Rev. Lett.* **2014**, *112*.
(24) Hohenberg, P.; Kohn, W. Inhomogeneous Electron Gas. *Phys. Rev.* **1964**, *136*, B864−B871.
(25) Runge, E.; Gross, E. K. U. Density-Functional Theory for Time-Dependent Systems. *Phys. Rev. Lett.* **1984**, *52*, 997−1000.
(26) Ramamoorthy, M.; Vanderbilt, D.; King-Smith, R. D. First-Principles Calculations of the Energetics of Stoichiometric TiO_2 Surfaces. *Phys. Rev. B* **1994**, *49*, 16721−16727.
(27) Enkovaara, J.; Rostgaard, C.; Mortensen, J. J.; Chen, J.; Dułak, M.; Ferrighi, L.; Gavnholt, J.; Glinsvad, C.; Haikola, V.; Hansen, H. A.; et al. Electronic Structure Calculations with GPAW: A Real-Space Implementation of the Projector Augmented-Wave Method. *J. Phys.: Condens. Matter* **2010**, *22*, 253202.
(28) Blöchl, P. E. Projector Augmented-Wave Method. *Phys. Rev. B* **1994**, *50*, 17953.
(29) Perdew, J. P.; Burke, K.; Wang, Y. Generalized Gradient Approximation for the Exchange-Correlation Hole of a Many-Electron System. *Phys. Rev. B* **1996**, *54*, 16533−16539.
(30) Stausholm-Møller, J.; Kristoffersen, H. H.; Hinnemann, B.; Madsen, G. K. H.; Hammer, B. DFT+U Study of Defects in Bulk Rutile TiO_2. *J. Chem. Phys.* **2010**, *133*, 144708−144708−8.
(31) Dudarev, S. L.; Botton, G. A.; Savrasov, S. Y.; Humphreys, C. J.; Sutton, A. P. Electron-Energy-Loss Spectra and the Structural Stability of Nickel Oxide: An LSDA+U Study. *Phys. Rev. B* **1998**, *57*, 1505−1509.
(32) Hammer, B.; Wendt, S.; Besenbacher, F. Water Adsorption on TiO_2. *Top. Catal.* **2010**, *53*, 423−430.
(33) Gavnholt, J.; Olsen, T.; Engelund, M.; Schiøtz, J. Δ Self-Consistent Field Method to Obtain Potential Energy Surfaces of Excited Molecules on Surfaces. *Phys. Rev. B* **2008**, *78*, 075441.
(34) Zawadzki, P.; Jacobsen, K. W.; Rossmeisl, J. Electronic Hole Localization in Rutile and Anatase TiO_2 − Self-Interaction Correction in Δ-SCF DFT. *Chem. Phys. Lett.* **2011**, *506*, 42−45.
(35) Ojanperä, A.; Havu, V.; Lehtovaara, L.; Puska, M. Nonadiabatic Ehrenfest Molecular Dynamics within the Projector Augmented-Wave Method. *J. Chem. Phys.* **2012**, *136*, 144103−144103−9.
(36) Qian, X.; Li, J.; Lin, X.; Yip, S. Time-Dependent Density Functional Theory with Ultrasoft Pseudopotentials: Real-Time Electron Propagation across a Molecular Junction. *Phys. Rev. B* **2006**, *73*.
(37) Castro, A.; Marques, M. A. L.; Rubio, A. Propagators for the Time-Dependent Kohn−Sham Equations. *J. Chem. Phys.* **2004**, *121*, 3425−3433.
(38) Meng, S.; Ren, J.; Kaxiras, E. Natural Dyes Adsorbed on TiO_2 Nanowire for Photovoltaic Applications: Enhanced Light Absorption and Ultrafast Electron Injection. *Nano Lett.* **2008**, *8*, 3266−3272.
(39) Burdett, J. K.; Hughbanks, T.; Miller, G. J.; Richardson, J. W. J.; Smith, J. V. Structural-Electronic Relationships in Inorganic Solids: Powder Neutron Diffraction Studies of the Rutile and Anatase Polymorphs of Titanium Dioxide at 15 and 295 K. *J. Am. Chem. Soc.* **1987**, *109*, 3639−3646.
(40) Morgan, B. J.; Watson, G. W. Intrinsic N-Type Defect Formation in TiO_2: A Comparison of Rutile and Anatase from GGA+U Calculations. *J. Phys. Chem. C* **2010**, *114*, 2321−2328.
(41) Kang, W.; Hybertsen, M. S. Quasiparticle and Optical Properties of Rutile and Anatase TiO_2. *Phys. Rev. B* **2010**, *82*.

(42) Henkelman, G.; Uberuaga, B. P.; Jónsson, H. A Climbing Image Nudged Elastic Band Method for Finding Saddle Points and Minimum Energy Paths. *J. Chem. Phys.* **2000**, *113*, 9901.
(43) Kowalski, P. M.; Meyer, B.; Marx, D. Composition, Structure, and Stability of the Rutile TiO_2(110) Surface: Oxygen Depletion, Hydroxylation, Hydrogen Migration, and Water Adsorption. *Phys. Rev. B* **2009**, *79*, 115410−115410.
(44) Zawadzki, P.; Laursen, A. B.; Jacobsen, K. W.; Dahl, S.; Rossmeisl, J. Oxidative Trends of TiO_2—Hole Trapping at Anatase and Rutile Surfaces. *Energy Environ. Sci.* **2012**, *5*, 9866−9869.
(45) Kerisit, S.; Deskins, N. A.; Rosso, K. M.; Dupuis, M. A Shell Model for Atomistic Simulation of Charge Transfer in Titania. *J. Phys. Chem. C* **2008**, *112*, 7678−7688.
(46) Becke, A. D.; Edgecombe, K. E. A Simple Measure of Electron Localization in Atomic and Molecular Systems. *J. Chem. Phys.* **1990**, *92*, 5397.
(47) Savin, A.; Nesper, R.; Wengert, S.; Fässler, T. F. ELF: The Electron Localization Function. *Angew. Chem., Int. Ed. Engl.* **1997**, *36*, 1808−1832.
(48) Marzari, N.; Mostofi, A. A.; Yates, J. R.; Souza, I.; Vanderbilt, D. Maximally Localized Wannier Functions: Theory and Applications. *Rev. Mod. Phys.* **2012**, *84*, 1419−1475.
(49) Calzado, C. J.; Hernandez, N. C.; Sanz, J. F. Effect of on-Site Coulomb Repulsion Term U on the Band-Gap States of the Reduced Rutile (110) TiO_2 Surface. *Phys. Rev. B* **2008**, *77*, 045118−045118.
(50) Wendt, S.; Sprunger, P. T.; Lira, E.; Madsen, G. K. H.; Li, Z.; Hansen, J. O.; Matthiesen, J.; Blekinge-Rasmussen, A.; Laegsgaard, E.; Hammer, B.; et al. The Role of Interstitial Sites in the Ti3d Defect State in the Band Gap of Titania. *Science* **2008**, *320*, 1755−1759.
(51) Tully, J. C. Molecular Dynamics with Electronic Transitions. *J. Chem. Phys.* **1990**, *93*, 1061−1071.
(52) Tapavicza, E.; Tavernelli, I.; Rothlisberger, U. Trajectory Surface Hopping within Linear Response Time-Dependent Density-Functional Theory. *Phys. Rev. Lett.* **2007**, *98*.
(53) Liu, L.-M.; Zhang, C.; Thornton, G.; Michaelides, A. Structure and Dynamics of Liquid Water on Rutile TiO_2(110). *Phys. Rev. B* **2010**, *82*.
(54) Henderson, M. A. Structural Sensitivity in the Dissociation of Water on TiO_2 Single-Crystal Surfaces. *Langmuir* **1996**, *12*, 5093−5098.
(55) Shevlin, S. A.; Woodley, S. M. Electronic and Optical Properties of Doped and Undoped $(TiO_2)_n$ Nanoparticles. *J. Phys. Chem. C* **2010**, *114*, 17333−17343.
(56) Martinez, U.; Vilhelmsen, L. B.; Kristoffersen, H. H.; Stausholm-Møller, J.; Hammer, B. Steps on Rutile TiO_2(110): Active Sites for Water and Methanol Dissociation. *Phys. Rev. B* **2011**, *84*.
(57) Gong, X.-Q.; Selloni, A.; Batzill, M.; Diebold, U. Steps on Anatase TiO_2(101). *Nat. Mater.* **2006**, *5*, 665−670.
(58) Shen, M.; Henderson, M. A. Identification of the Active Species in Photochemical Hole Scavenging Reactions of Methanol on TiO_2. *J. Phys. Chem. Lett.* **2011**, *2*.
(59) Phillips, K. R.; Jensen, S. C.; Baron, M.; Li, S.-C.; Friend, C. M. Sequential Photo-Oxidation of Methanol to Methyl Formate on TiO_2(110). *J. Am. Chem. Soc.* **2013**, *135*, 574−577.